REMOTE SENSING IN THE NEVA BIGHT

Friedwart Ziemer[1], Carsten Brockmann[2], Robin A. Vaughan[3] and Alexander Barkatov[4]

1. GKSS Research Centre Geesthacht, Institute for Coastal Research, 21502 Geesthacht, Germany; ziemer(at)gkss.de
2. Brockmann-Consult, 21502 Geesthacht, Germany; brockmann(at)brockmann-consult.de
3. University of Dundee, Dundee, DD1 4HN, UK; r.a.vaughan(at)dundee.ac.uk
4. Electrotechnical University, St. Petersburg, Russia; aleksbar(at)yandex.ru

ABSTRACT

The recently completed HYMNE project (Hydrographic Monitoring of the Neva Bight) was designed specifically to provide the scientific basis for an operational hydrographic monitoring system as a management tool for preserving the ecological and economic resources of the hydrosphere within the metropolitan region of St Petersburg and the neighbouring parts of the Baltic Sea. It was an INCO/Copernicus project involving scientists from Germany, UK, Finland, and Russia. This paper concentrates on the incorporation of an innovative component into the system, which is the ground-based radar providing data on a high resolution grid. It was one of the main thrusts of the HYMNE project to develop and test such a system. In addition, sea truth and satellite measurements were undertaken as well as an in-depth study of the environmental impact of the river discharge into the Eastern Gulf of Finland/Neva Bight region. Of particular interest was the effect of the newly constructed flood protection barrier on the circulation and mixing of the river and gulf waters.

Keywords: Hydrographic monitoring, ground based Doppler radar, surface current

INTRODUCTION

Two ground-based X-band radars were used to detect hydrodynamic parameters such as the surface current during the ice-free season, and floe mobility under winter conditions. The radar was mounted on the shore close to the shipway's barrier opening. It was shown that the sea surface current can be calculated from the radar signal Doppler shift detected from two positions (Figure 4). For this purpose, the frequency shift acquired from each individual position must be corrected for the effects due to the local wind and wave impact (1). The radial components from two stations were combined to obtain a map of sea surface current vectors. To observe the floe mobility, time series of the radar images were Fourier decomposed. Arial structures due to stationary ice fields were recognised to induce a signal with zero frequency. Signals with nonzero frequencies were detected over moving ice fields.

In addition to the ground-based radar measurements both SAR and optical satellite data were analysed. The period of research coincided with the end of the lifetime of ERS 2, and so only a limited number of SAR scenes were available, none during the fieldwork campaigns. The 35-day repeat cycle was too long to obtain any useful information on water and ice-floe movements, but did provide periodic overviews of the general situation. Little previous work has been done using SAR in shallow, polluted, turbid river basins where it is difficult to separate the scattered signal of ice from that of water, but some algorithms were developed which would, in principle, yield information about the ice type, pollutant concentration and liquid water equivalent, if sufficient temperature and salinity *in situ* data were available (2).

Optical data from SeaWiFS, from the NASA data archive, and AVHRR, provided by the German Federal Maritime and Hydrographic Agency, were analysed for the period May 1998 to September 2000. About 20 cloud-free SeaWiFS and 121 AVHRR images were available for this period. The turbidity pattern derived from SeaWiFS could be related to the typical algae distribution in the Gulf of Finland and to the suspended sediment pattern in the Neva Bight. Some phenomena from sin-

gle days were observed, particularly those associated with the water passing through the barrier, and the distribution of chlorophyll in the eastern end of the Gulf. However, due to the limited number of images, it was not possible to provide a statement concerning a regular pattern of the river currents. Seasonal sea surface temperature patterns were also studied by calculating mean and standard deviations in ten different areas and related to available *in situ* data. Statistically significant relationships between the water masses at the barrier and the surrounding waters were derived.

DETECTION OF A CURRENT VECTOR FIELD

The Doppler measurement is based on the phase detection of the individual radar beam. For each range bin from the complex signal of two succeeding time steps $\Im(r,t_i)$ and $\Im(r,t_{i+1})$ the phase difference $\Delta\varphi$ is detected. From this the radial velocity component can be deduced by:

$$v_{radial}(r_i,t) = \frac{\lambda_{radar}}{2}\frac{\Delta\varphi}{2\pi\,\Delta t} \qquad (1)$$

where: $\Delta\varphi = \varphi_2 - \varphi_1$, $i=1,2,...N$,

	v_{radial}	radial movement of the back scattering surface element (bin),
	N	number of range bins,
	r_i	radial distance of bin i,
	λ_{radar}	length of electromagnetic wave,
	φ_1	angle of phase in complex radar back scatter at distance r_i and at time t_1,
	φ_2	angle of phase in complex radar back scatter at distance r_i and at time t_2,
and	Δt	time step between transmissions of two radar pulses.

Eq. (1) denotes the physical relation to deduce the relative radial movement of each radar backscattering surface element by the phase shift between two successive radar signals. Eq. (1) contains the Doppler frequency shift of the back scattered radar frequency, which is:

$$f_{Doppler} = \frac{1}{2\pi}\frac{\Delta\varphi}{\Delta t} \qquad (2)$$

The radar was operated with 1000 transmission pulses per second, Δt = 0.001 s. The radar used is an X-band system with an electromagnetic wavelength of λ_{radar} = 3 cm. For the time of data acquisition (T = 10 s) the view direction of the radar antenna was fixed. As the radar backscatter from the sea surface carries a large amount of noise, the total data set was subdivided into a series of ten subsequent samples each of which was spectrally analysed. The resulting Doppler spectra covering the bandwidth from 1 to 500 Hz with a resolution of 1 Hz were used to detect the actual frequency shift. Averaging the spectra of the sequence of samples provides significant values, which can be assumed to be representative for the quantities of interest for v_{radial}.

CONTRIBUTIONS TO RADIAL VELOCITIES

To interpret the radial movement within a radar backscatter cell detected under the use of Eq. (1), we will first discuss the three main effects which contribute to this movement. These are: i) the phase speed of the short waves backscattering the electromagnetic waves, ii) movement of the water surface layer due to the local impact of the wind friction and iii) the periodic movement of the long wave field.

Radar backscatterers

The physics of radar backscattering is described by the Bragg scattering effect. This effect, discussed for grazing incidence in (1), describes the interaction of the electromagnetic waves with that part of the sea surface waves which are in resonance with the radar waves. The condition of

resonance is: $k_{scatterer} = 2k_{radar}\cos\psi$, where $k_{scatterer} = 2\pi/\lambda_{scatterer}$ is the wave number of that component within the sea surface roughness fulfilling the resonance condition with $k_{radar} = 2\pi/\lambda_{radar}$. The argument ψ is the local angle of incidence of the radar signal. As ψ is close to grazing this indicates that the radar selects one particular wave from the full spectrum of waves which composes the sea surface roughness. Thus, this wave has the length: $\lambda_{scatterer} = \frac{1}{2}\lambda_{radar}$.

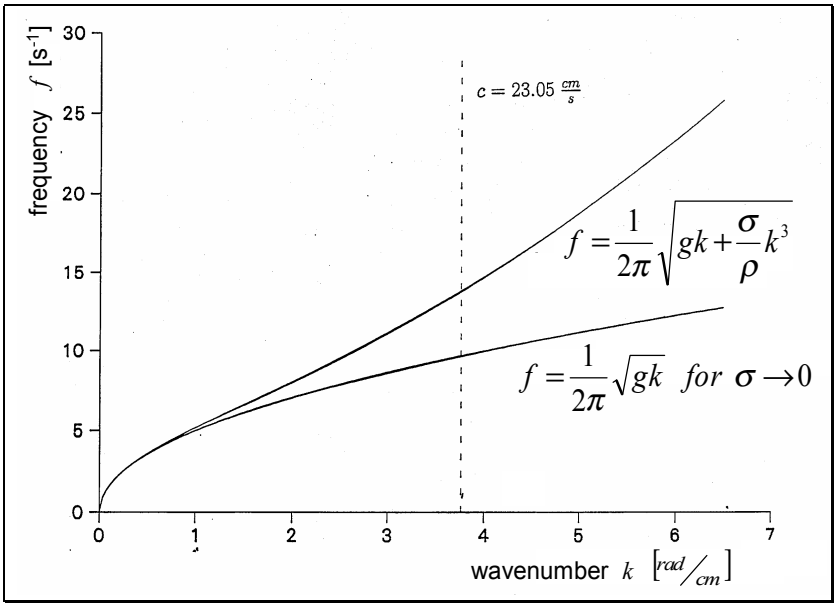

Figure 1: Dispersion relation describing the functional dependence of the wave number and the frequency. The transient frequency bandwidth covering gravity waves (lower curve) to capillary waves (upper curve) with surface tension under slick free condition is shown. The dashed line marks the wave number with the wave length $\lambda_{scatterer}$ = 1.5 cm which at grazing incidence corresponds to the radar wave length of 3 cm for a 9 GHz transmission frequency.

Figure 1 shows the isotropic dispersion relationship for a broad spectrum of sea surface waves. As balancing forces we consider the gravity due to earth acceleration and the surface tension which is active for short waves whose lengths are less than some centimetres.

$$\omega = \sqrt{gk + \frac{\sigma}{\rho}k^3}\ .$$

Here g is the earth acceleration, σ the surface tension, and ρ the density of the water. For this relation isotropy is valid as long as no directional dependency is active. The phase speed of the scatterers

$$c = \sqrt{\frac{g}{k_{scatterer}} + \frac{\sigma}{\rho}k_{scatterer}}\ . \qquad (3)$$

is determined by the radar frequency.

Orbital velocities

The propagation of long waves causes an oscillation of the near surface water particles around their positions of equilibrium. Considering an individual wave component with the wave height H the particles describe the circle with the radius: $r_o = H/2$. From this, the velocities at the sea surface can be derived as follows from:

$$v(z)\big|_{z=0} = v_o = \frac{2\pi r}{T} = \frac{\pi H}{T}\ . \qquad (4)$$

From typical values during data acquisition for the wave heights (*H = 0.5 m*) and the wave periods ($T = 3\,\mathrm{s}$) it follows that values for the orbital movements are of the order $v_o \approx 0.5\,\mathrm{m/s}$.

Surface wind friction velocity

As during our experiments the wind speed did not exceed $u_{10} \leq 6\ \mathrm{m/s}$, we consider the impact by the wind on the signal Doppler shift to be sufficiently described via the surface stress**:**

$$\tau = \rho_{air} u_*^2 \tag{5}$$

with: ρ_{air} density of air

and $u_* = \sqrt{c_D}\, u_{10}$ friction velocity at the sea surface.

In Eq. (5) the drag coefficient c_D is included.

Estimate of current velocity

For the given purpose, to estimate the amount of water transport through the gate, the sea surface current vector has to be detected. The radial results must be corrected for the effects discussed above. As the scattering wavelength is the same for each measurement, and as the change of the angle of incidence is small enough to be omitted, we set the phase speed of the backscatterers to a constant value: $c = 23\,\mathrm{cm/s}$. But as we observe the radial component we have to take into account the directionality of this value and define the phase speed to be a vector: $\vec{c} = (c_x, c_y)$. To estimate the additional influence of the wind friction velocity we make a first guess by assuming stable conditions thus pre-setting the drag coefficient to be $c_D = 1{,}3 \cdot 10^{-3}$. For the value of the friction velocity this results in approximately 3% of the wind speed at 10 m height. Thus we assume: $u_* \approx 0.03\, u_{10}$. Neglecting local wind changes we assume for the direction of u_* the same direction as for the wind vector measured at the location of the radar station.

To reduce the influence of the orbital movements due to long waves the averaging time was chosen to cover the dominant wave T_z at least two times. During the experiments the longest wave period observed was $T_z = 3$ s. As the total observation time was set to $T_{Observation} = 10\,\mathrm{s}$, the mean wave period was covered by samples even more than three times. For each range bin one gets from Eqs. (1) and (2) the relative, radial speed at the time instant t_1:

$$v_{radial}(t)\big|_{t=t_1} = \frac{\lambda_{radar}}{2} \frac{1}{2\pi} \frac{\Delta\varphi}{\Delta t} = \frac{\lambda_{radar}}{2} f_{Doppler} \tag{6}$$

Figure 2 shows the scheme for geo-coding the collocation points of two radar rays from the GPS positions and the ranging of each of the radars. The North orientation was deduced from the bearing (North orientated azimuth) between the two stations. From this the position of each point relative to both radars is known.

The wind condition during the radar observation was observed with 4 m/s from 210°. The measured Doppler shifts from each of the radars were transferred to radial surface speeds by Eq. (6), corrected by the wind friction (Eq. 5) and by the phase speed of the scatterers. By collocating the results of the two radars the surface current vector field was composed into an Eulerian grid (see Figure 4). The length of each arrow gives the current speed and the direction corresponds to the North orientated current direction. The dotted arrows result from Doppler spectra with multiple peaks, indicating uncertain measurements.

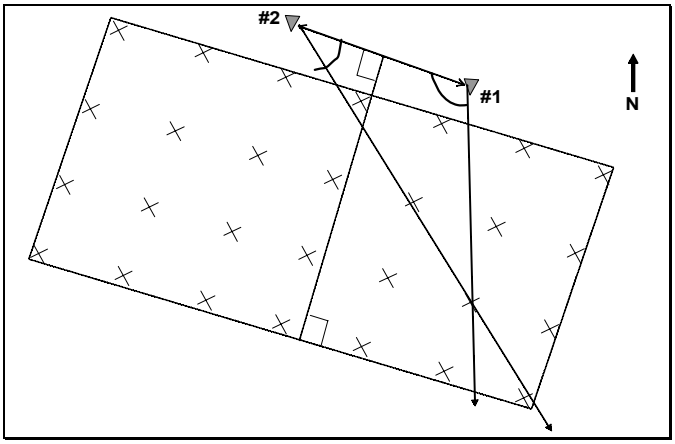

Figure 2: Geo-coding of the collocation points of two radars at the positions #1 and #2 by using the GPS positions of each of them. The North orientation was deduced from the bearing between the two stations.

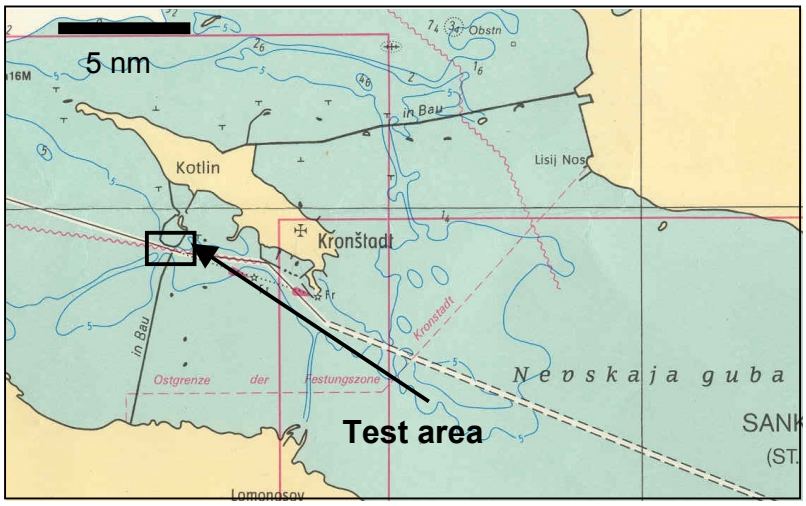

Figure 3: The position of the observation area south of the island "Kotlin". The sea chart (BSH) shows the storm protection dyke closing the Neva Bight at its West end. The radar stations were located at the North side of the opening for the ship way.

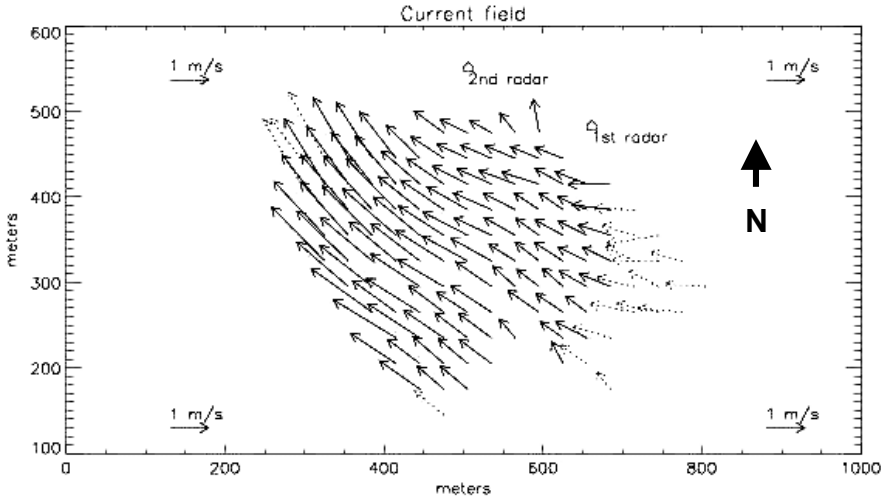

Figure 4: Corrected surface current vector field presented in an Eulerian grid. The lengths of the arrows give the current speed and the arrows direction corresponds to the North orientated current direction. The observation area is the ship's gate marked in the map, Figure 3. The dotted arrows result from Doppler spectra with multiple peaks, indicating uncertain measurements.

The observed current vector field shows a situation during which the outflow of the river Neva controls the regime. The directions indicate that the flow is guided by the bathymetry (Figure 3), that is characterised by the ship's channel crossing the storm protection dyke south of the radar stations.

CONCLUSIONS

It was shown for the first time in the HYMNE project that the ground-based radar has the potential to deliver high resolution information on the local current field, on ice-flow mobility, and an estimate for the water transport rates within a spatial window of some km^2. Thus a valuable tool for the monitoring of a semiclosed hydrosphere will be achieved, if additional calibration and verification of this technique are conducted. The ground-based radar has a high potential to close the gap between the sparsely available satellite and *in situ* observations and to provide a continuous and direct reporting to a data collection centre to which decision makers may have access.

ACKNOWLEDGEMENTS

The authors would like to thank Dr. Sergey Kalenichenko and the radar group at the Electrotechnical University St. Petersburg for mounting and operating the radar and for data acquisition. This work was co-funded by the European Commission under the contract: ICA2-CT-2000-10034 HYMNE.

REFERENCES

1 Trizna D B, 1985. A model for Doppler peak spectral shift for low grazing angle sea scatter. IEEE Journal of Oceanic Engineering, OE-10, 368-375

2 Djepa V, 2002. Microwave Remote Sensing of Ice Concentration and Windspeed. MSc thesis, University of Dundee.